Development of an adequate model for verification of design safety-margins of the HTTR nuclear test facility

Alain FLORES[a,*], José María IZQUIERDO[b], Miguel SÁNCHEZ-PEREA[b] and Eduardo GALLEGO[a]

[a] *Nuclear Engineering Department - Universidad Politécnica de Madrid, José Gutiérrez Abascal 2, 28006 Madrid, Spain*

[b] *Departamento de modelación y simulación – Consejo de Seguridad Nuclear, Justo Dorado 11, 28040 Madrid, Spain*

This work is based on the prototype High Engineering Test Reactor (HTTR) of the Japan Agency of Energy Atomic (JAEA). Its objective is to describe an adequate deterministic model to be used in the assessment of its design safety margins via damage domains. The concept of damage domain is defined and it is shown its relevance in the ongoing effort to apply dynamic risk assessment methods and tools based on the Theory of Stimulated Dynamics (TSD). To illustrate, we present results of an abnormal control rod (CR) withdrawal during subcritical condition and its comparison with results obtained by JAEA. No attempt is made yet to actually assess the detailed scenarios, rather to show how the approach may handle events of its kind.

KEYWORDS: HTTR, dynamic reliability, modelling, high temperature gas reactor, simulation, damage domain

[*]Corresponding author. Tel.:+34 913363112 E-mail address: alain.floresy@gmail.com

1. Introduction and purpose

1.1 Introduction.

1.1.1 The HTTR facility.

The HTTR facility explores the advantages and efficiency of high-temperature helium gas reactors for hydrogen generation (in conjunction with production of conventional thermal power), based on nuclear power. The high temperature gas may be used in hydrogen production facilities, like for instance in the concept of the RAPHAEL project (Hittner et al., 2006) and some reactors of the GEN IV (GIF, 2002).

HTTR includes a graphite moderated, helium gas-cooled reactor with a thermal power of 30 MW and a reactor coolant outlet temperature of 950ºC (Saito et al., 1994).
The reactor cooling system consists of a primary cooling system (PCS), a secondary helium cooling system (SHCS), a pressurized water cooling system (PWCS) and a vessel cooling system (VCS), as schematically shown in **Fig. 1**.

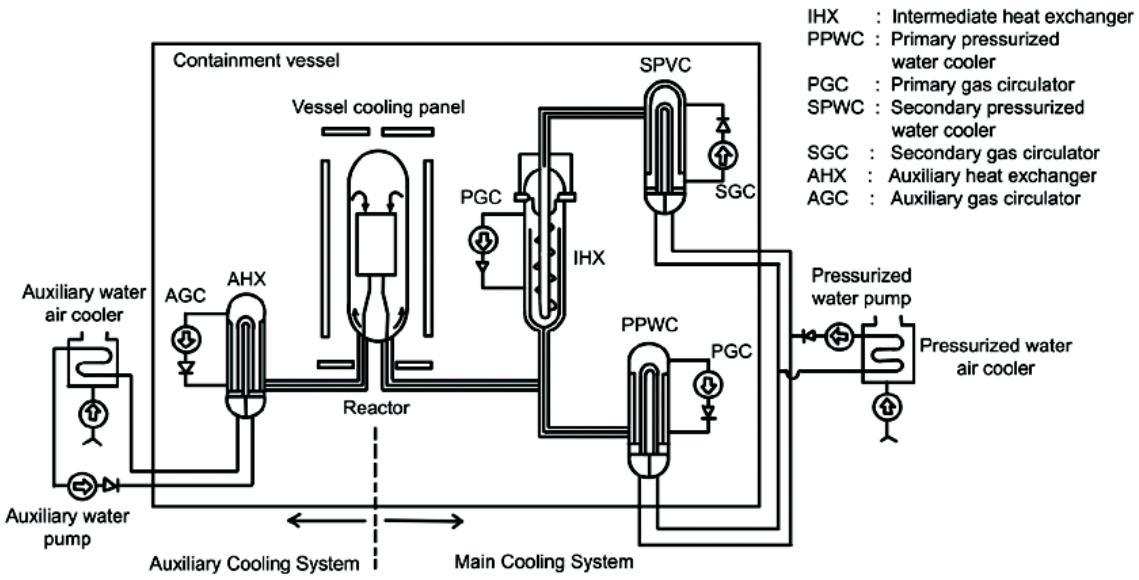

Fig. 1. Reactor cooling system of HTTR (Saito et al., 1994).

1.1.2 Safety design features

As it is customary, and as indicated in its safety analysis report (Saito et al., 1994), the HTTR design use standard deterministic safety assessment techniques to ensure that a carefully defined Design Basis Envelop (DBEP), groups actual transients in design categories such that protections envisaged for representative transients of the different categories are adequate enough.

By this it is meant that any of the actual transients that may really occur will have no worse consequences as those anticipated by the study of the representatives of each DBEP category, henceforth called design basis transients. Consequences are characterized by the damage that may be generated, defined as a given function of process variables (damage indicators) exceeding specified allowed limits (hereafter safety limits) during its time evolution.
In **Table 1** the safety limits of concern are specified

Table 1 Acceptance criteria for anticipated operational occurrence (AOO) for the HTTR (Kunitomi et al., 2004)

- The peak fuel temperature shall be less than 1600 ºC
- Pressure on reactor pressure boundary is less than 1.1 times of maximum pressure in service (<5.28 MPa).
- Maximum temperatures of reactor pressure boundary

  9/4Cr-1Mo steel<500 ºC

  Austenitic stainless steel<600 ºC

  Hastelloy XR<980 ºC

1.2. Purpose

Given the complexity of interactions between protection actions, phenomena, and dynamic processes, it becomes difficult to verify that indeed the acceptance criteria are met. A new

approach to tackle this and other issues related with potentially undue grouping, due to dynamic, features has been developed within the regulatory space of the Nuclear Industry. It is based on the Theory of Stimulated Dynamics (TSD) and includes a risk assessment methodology as well as a platform of simulation tools for its implementation (Izquierdo and Cañamon, 2008; Izquierdo and Cañamón, 2006; Izquierdo et al., 2008; Labeau and Izquierdo, 2005a, b; Sánchez et al., 2009), all together named TSD.

We call "damage domain" of a given safety limit the region of the space of uncertain and sensitive parameters of interest where the limit is exceeded. The damage domain of the DBEP transients should be empty, so no design transient should violate design safety limits for any of the transients included in its categories. However, the examination of the damage domains sensitivity to the safety limits is of paramount interest for the quality of the design.

The main objective of this and subsequent papers is to generate the HTTR damage domains and assess its safety margins on some of the HTTR design basis events, namely anticipated operational transients (AOO). This first contribution describes the model and code used for damage domain identification and presents some test results on overpower transients. Further details of the relation between damage domains and safety margins are described below.

2. - Main characteristics of TSD methods. Damage domains and safety margins

A key issue in the safety assessment is to verify the adequacy of the HTTR specified maximum allowed initial conditions (LCO, limiting conditions for operation) as well as the design of their set points for safeguard initiation signals (LSSS, limiting safety system settings). **Table 2** specifies those relevant for our case study.

In **Table 2** and **Table 3** the expected safeguard action events are shown with an indication of

the set points for its automatic initiation (Saito et al., 1994).

Table 2 Safeguards considered available in the AOO- HTTR safety assessment (Saito et al., 1994)

Systems or components	AOO
Reactor Protection system	X
Control Rod (CR) system	X
Auxiliary Cooling System (ACS)	X
Vessel Cooling System VCS	X
Emergency power feeder	X
Frequency converter of Primary Gas Circulator (PGC)	X
Pressurized water pump trip by means of high temperature of PWCS inlet pressurized water	X

Table 3 Signals of reactor scram (Saito et al., 1994)

Signal of reactor scram	Established value	
Reactor power at PRMS	High	105.5%
Primary coolant flow rate of IHX	Low	92%
Primary coolant flow rate of PPWC	Low	93%
IHX outlet temperature	High	410ºC
Reactor outlet coolant temperature	High	967ºC
Core differential pressure	Low	78%
Pressurized water flow rate PPWC	Low	87%
Differential pressure between PCS and PWCS	High	8.5 kg/cm^2
Differential pressure between PCS and PWCS	Low	1.5 kg/cm^2
Differential pressure between PCS and SHCS	Large	1.8 kg/cm^2

Secondary helium flow rate	Low	88%
Manual scram	------	------

In the TSD context, each possible transient, resulting from a given accident initiator and LCO conditions, when different combinations of safeguard initiation set points are reached, is called a path. Paths are grouped in dynamic sequences defined as the set of all transients that have activated the same settings, but differing in its timing. A path is then characterized by a set of times within the same dynamic sequence.

When considering the LCO and LSSS parameters, its uncertainty should also be included in the assessment. To each path we associate the joint probability of those parameters, and the probability aggregate for all transients in the damage domain become the conditioned probability of damage relative to the initiator. When multiplied by the frequency of the initiator we get the frequency of exceedance of the safety limit, which is the main figure of merit in the TSD verifications. For instance, when considering a safety limit more restricted than the one required, the frequency of exceedance corresponding to the damage domain obtained gives an indication of safety margins and its sensitivity to the settings.

2.1. Identification of damage domains. Adequate deterministic models

The calculation of the exceedance frequency of a given safety limit, main figure of merit to verify the regulatory or design risk limits, is then a two-fold task: (1) damage domain identification, i.e. the set of all possible damage transients grouped in a sequence, and (2) computation of the exceedance frequency sensitivity to the safety limits i.e. the safety margins.

As indicated above, a damage domain of a given safety limit is the locus in the space of uncertain parameters where the limit is exceeded. The damage domain is then a volume in the

multi-dimensional space of times and parameters, each point in it representing a different transient. As a result, a large amount of transients are to be simulated, thus making the model to simulate everyone a work-horse essential to TSD application. Indeed, other analysis of similar scenarios related to NPP safety, promote simplified and fast resolution models (EPRI, 2011; Izquierdo et al., 2001).

Because the quantities to be aggregated are positive, it is obvious that if a damage domain including another is used, the resultant damage frequency will also be higher than that obtained with the included one. This means that we can use lower fidelity models to reduce first the very large amount of transients to be covered, improving the model fidelity and detail in successive iterations such that the larger the domain the lower the need for detail, provided it can be proved and /or checked that no success path damage found with a lower fidelity model turns out to be a damage path if simulated with a higher fidelity one. In view of the large dimensions of the damage domain this approach is basically inevitable. We focus here in finding a first iteration adequate model, the adequacy criterion judged as above.

3. HTTR model for AOO transients with main coolant pumps working

3.1 Relevant HTTR design and operation features

As can be seen in **Fig. 1**, the primary cooling system (PCS) is constituted by the main cooling system (MCS) and auxiliary cooling system (ACS). The MCS has two heat exchangers: a helium-helium intermediate heat exchanger (IHX) and a primary pressurized water cooler (PPWC). Primary helium gas is transported from the reactor core to the IHX and PPWC through a primary concentric hot gas duct.

The secondary helium cooling system (SHCS), mainly consisting of the secondary pressurized water cooler (SPWC), removes the heat from the primary helium gas through the

IHX.

The primary water cooling system (PWCS) consists of an air cooler, water pump and so on. An air cooler cools the pressurized water in both the PPWC and SPWC and transfer the heat from the reactor core to the final heat sink of atmosphere.

The ACS is standby during normal operation and starts up to remove the residual heat after a reactor scram.

The vessel cooling system (VCS) runs at rated flow rate during normal operation to cool the biological concrete shield.

It cools the reactor under a no forced-cooling condition such as a primary pipe rupture accident when the ACS is no longer able to cool the core effectively.

The schematic block diagram of the different cooling loops is represented in **Fig. 2**. Further details of the system are described in (Saito et al., 1994)

Fig. 2 shows the block diagram of the different cooling loops locating the five main regions of the main reactor cooling system. For transients working in an operating mode with the IHX out of service, as the case example analyzed below, only these regions are modelled. If in emergency operation mode with only the auxiliary helium exchanger (AHX) pumps operating, a similar cooling loop involving the core and AHX loop is the one of interest. For parallel, at power operation, the IHX secondary helium circuit is included with a similar treatment. Thus, the basic module for simulation is a five region loop model.

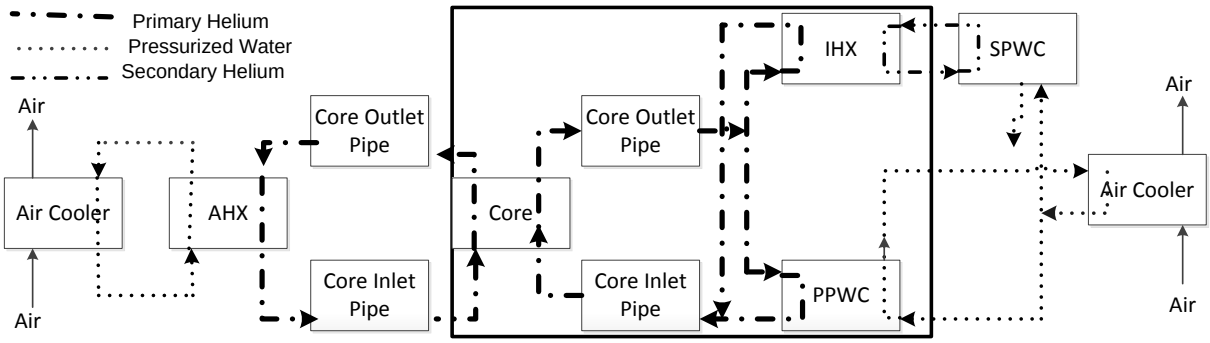

Fig. 2. Schematic diagram of the reactor cooling system of HTTR.

3.2 Simulating abnormal operational transients. The GASTEMP/HTTR code

Below we describe general aspects of our GASTEMP/HTTR5 code model, called that way because it considers only one region at each of the five loop sections of the main module, and it is further simplified by using a high velocity approximation of the thermal-fluid conservation equations (see appendix A). All data are the same as those used in the JAERI ACCORD code (Takeda et al., 2000). Properties of the fuel, moderator and coolant are also taken from HTTR sources (Fujimoto et al., 2004; Iyoku et al., 2004; Saito et al., 1994; Sumita et al., 2004; Takeda et al., 2000).

3.2.1 The GASTEMP/code

GASTEMP (Benikhlef et al., 2011; Izquierdo and Sanchez, 2007) was developed to account for the enthalpy and mass balances of a time varying volume that includes a mixture of non-condensable and condensable gases. The volume may be heated by an external source and/or by internal chemistry reactions.

In our case there is just a single, non-reacting gas, but with a sophisticated external heat flux like the reactivity-fed nuclear heat flux described in section 4.3 below. The heat flux is computed by the HTTR5 sub-code, as described below. In appendix B, we also provide additional details about the coupling of both codes.

It may be easily shown that **Eqs.** A-6 and A-10, main implication of the high velocity loop assumption, lead to a special application of the energy and mass balances that are the basis of GASTEMP, that uses standard ordinary differential equations (ODE) solvers. We have then adapted GASTEMP to incorporate solutions of the nuclear and heat exchanger heat-flux models like those described in section 4. Instead of a single volume, we now have five main volumes connected through the volumetric flows as described in **Eq.** A-13.

The extra methods required for the GASTEMP-HTTR adaptation are then limited to add the solvers for the heat flux equations of type B.5 and connect the five volumes, speeding up the rest of the code.

In summary, GASTEMP/HTTR5 is an adaptation of the GASTEMP code to solve the set of equations that describe the five sections module of the HTTR cooling loops, as described in the follow sections.

4. The HTTR core-heat transfer code

4.1. Neutron power. The point model.

A single group point-kinetics model is used, the model constants obtained from the ACCORD data (Takeda et al., 2000)

$$\dot{n} = \left(\frac{\rho - \beta}{\Lambda} \right) n + \lambda C + q \,, \quad \dot{C} = \frac{\beta}{\Lambda}\, n - \lambda\, C \qquad (1)$$

4.2 Decay heat power

The model for decay heat of fission products after reactor scram, is also following the ACCORD approach for fission products and actinide decay heat.

$$\frac{P_d}{n_d}+\frac{P_{act}}{n_d}=\frac{1}{Q}\sum_j A_j t_s^{-B_j}\theta_j+\frac{RE_U}{Q}\exp(-\lambda_u t_s)+\frac{RE_{Pu}}{Q}\frac{\lambda_u\exp(-\lambda_u t_s)-\lambda_{pu}\exp(-\lambda_{pu}t_s)}{\lambda_u-\lambda_{pu}} \qquad (2)$$

Parameters A and B depend on the elapsed time after scram, t_s, and are shown in **Table 4**.

θ_j is 1 if in interval $t_{j-1}<t_s<t_j$ and zero otherwise

Table 4 Decay heat parameters in Shure's formula (Takeda et al., 2000)

t_s(s)	A	B
$0.1\le t_s<10$	12.05	0.0639
$10\le t_s<150$	15.31	0.1807
$150\le t_s<4x10^6$	26.02	0.2834
$4x10^6\le t_s<\infty$	53.18	0.335

To simplify the description, in the following we will not consider the decay heat, that is however included in the code as an additional heat source.

4.3 Reactivity feedback

It takes into account the reactivity coefficients of the HTTR (Saito et al., 1994; Takeda et al., 2000). The total reactivity is $\dot{\rho}=\sum\frac{\partial\rho}{\partial x}\dot{x}=\frac{\partial\rho}{\partial T_f}\frac{\partial T_f}{\partial t}+\frac{\partial\rho}{\partial T_v}\frac{\partial T_v}{\partial t}+\frac{\partial\rho}{\partial Z_{bc}}\frac{\partial Z_{bc}}{\partial t}$ (3)

Fig. 3 and **Fig. 4** show the Doppler feedback and the moderator reactivity coefficient.

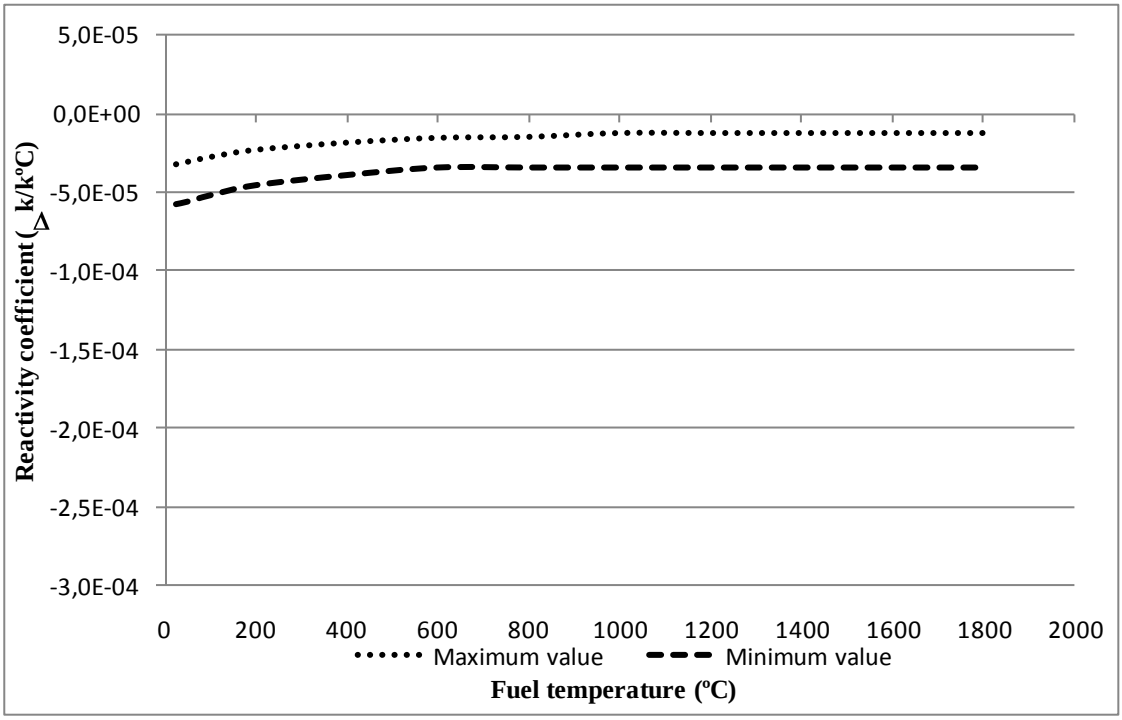

Fig. 3. Doppler coefficient.

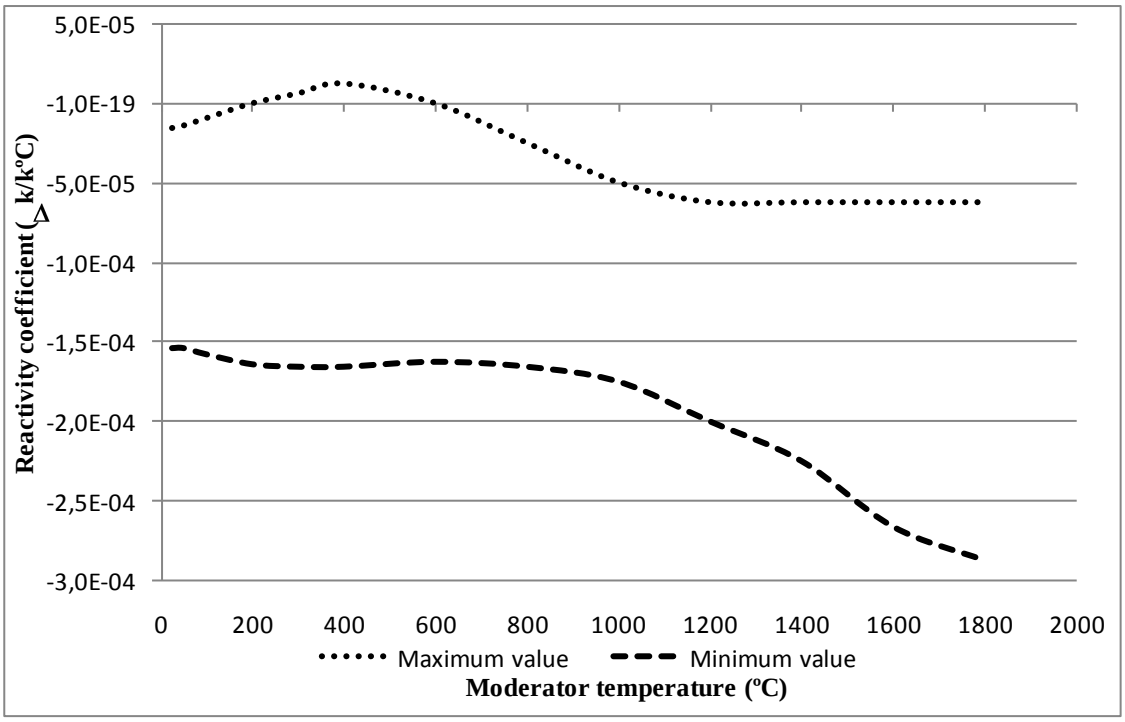

Fig. 4. Moderator temperature coefficient.

4.4 Core heat transfer: heat flux to the coolant

For the heat transfer from the fuel to the coolant, we choose a classical simple model accounting for different thermal resistances for each node, as shown in **Fig. 5:** left side for the fuel compact and right side for the transfer tube of the heat exchangers.

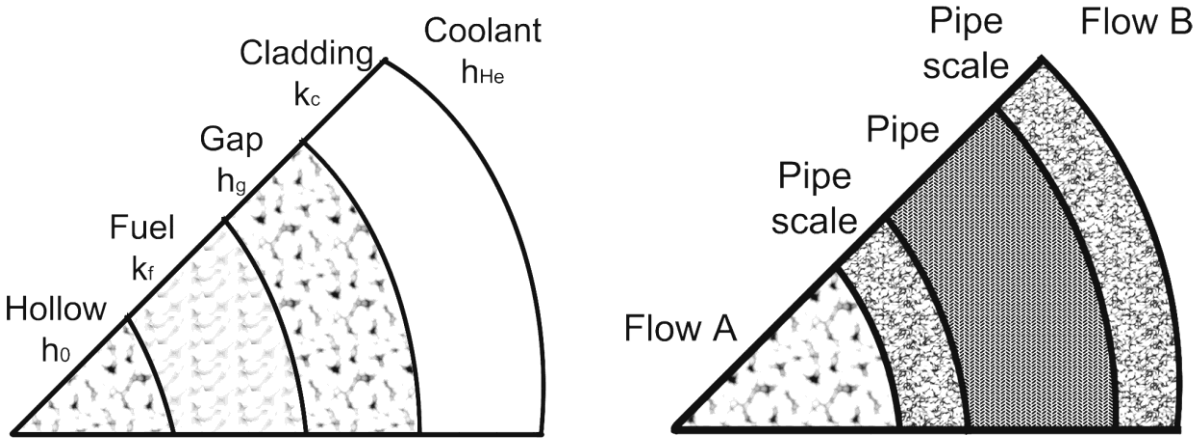

Fig. 5. Cross section of a fuel element and heat transfer tube.

The heat flux transmitted between two consecutive layers, for instance cladding, v, and fluid, He, is

$$\phi_{vc} = \frac{T_v - T_{He}}{R_v} \qquad \phi_{nf} = n(t) \tag{4}$$

and the heat balance is (residual heat not included)

$$\dot{T}_f = \phi_{nf} + \phi_{fv} = -\frac{1}{C_f \;\; R_f + R_g} T_f + \frac{1}{C_f \;\; R_f + R_g} T_v + \frac{1}{C_f} n \tag{5}$$

$$\dot{T}_v = \phi_{fv} + \phi_{vHe} = \frac{1}{C_v \;\; R_f + R_g} T_f - \frac{R_v + R_f + R_g}{C_v R_v \;\; R_f + R_g} T_v + \frac{1}{C_v R_v} T_{He} \tag{6}$$

where we have incorporated the gap conductance R_g assumed to be small enough as to have zero heat capacity.

If the core is divided in n-core nodes then

$$n_j(t) = \alpha_j n(t) \qquad \sum_{j=1,ncore} \alpha_j = 1 \tag{7}$$

with α_j the fraction of neutron power generated in node j.

5. Main cooling loop mass and energy conservation equations.

5.1 Heat exchangers region heat transfer.

An entirely similar approach is used in the heat exchangers, where equations 5 to 7 are also used according to **Fig. 5** right.

Because the water circuit has a pressure control, it is assumed that its temperature is kept in steady state, so the transient modelling considers it as a steady heat sink temperature. This heat exchanger water steady state, may also be divided in Nhex axial nodes with a steady water temperature $T_{wj} = hex_j T_w^{in}$ with coefficients hex_j computed at steady state conditions. The assumption of an average heat capacity of the metal and fluid may be used as an option, particularly in global balances.

5.2 Main cooling loop global balances

Without loss of generality we assume an operation mode where the loop mass is kept constant. According to **Eq** A.8 of appendix A, the loop global balance reads in this case

$$M^{loop} = G\tau_{loop} \qquad M^{loop}\frac{dh_j^{loop}}{dt} = \phi_{\nu\,He}^{loop} + \phi_{He\,w}^{loop} \qquad \phi_{\nu\,He}^{loop} = \frac{T_\nu - T_{He}^{loop}}{R_\nu} \tag{8}$$

$$\phi_{He\,w} = -U(T_{He}^{loop} - T_w) \quad U \equiv \frac{1}{R_{He\,t}} + \frac{1}{R_{t\,w}} \tag{9}$$

and the system composed by **Eq** (1), **Eq**. (2), **Eq**. (3), **Eq**.(4) and **Eq**. (9) can be represented as,

$$\begin{bmatrix} \dot{n} \\ \dot{C} \\ \dot{T}_f \\ \dot{T}_v \\ \dot{T}_{He} \end{bmatrix} = \begin{bmatrix} \frac{\rho-\beta}{\Lambda} & \lambda & 0 & 0 & 0 \\ \frac{\beta}{\Lambda} & -\lambda & 0 & 0 & 0 \\ \frac{1}{C_f} & 0 & -\frac{1}{C_f\ R_f+R_g} & \frac{1}{C_f\ R_f+R_g} & 0 \\ 0 & 0 & \frac{1}{C_v\ R_f+R_g} & -\frac{R_v+R_f+R_g}{C_vR_v\ R_f+R_g} & \frac{1}{C_vR_v} \\ 0 & 0 & 0 & \frac{1/R_v}{GC_p\tau} & -\frac{1/Rv+UA}{GC_p\tau} \end{bmatrix} * \begin{bmatrix} n \\ C \\ T_f \\ T_v \\ T_{He}^{loop} \end{bmatrix} + \begin{bmatrix} 1 & 0 & 0 & 0 & 0 \\ 0 & 0 & 0 & 0 & 0 \\ 0 & 0 & 0 & 0 & 0 \\ 0 & 0 & 0 & 0 & 0 \\ 0 & 0 & 0 & 0 & \frac{UA}{GC_p\tau} \end{bmatrix} * \begin{bmatrix} 0 \\ 0 \\ 0 \\ 0 \\ T_w \end{bmatrix} \quad (10)$$

As a result of the global balance the loop heat flux $\dot{Q}^{loop}\ \ t\ = \phi_{v\ He}^{loop} + \phi_{He\ w}^{loop}$ is determined.

5. 3 Mass and energy regional balances

In appendix A we describe the basis for the following mass and enthalpy balances at high speed in loops. They take into account that the gas coolant experiences significant expansion/contraction due the heating/cooling flux, so the volumetric flow j(z,t) (velocity) is quite different at the entrance of each of the four regions described above. A general volume conservation equation (see section 6.1 below) was also used.

Region j enthalpy balance

$$m_j^{reg}\ \frac{d}{dt}\left[h_j^{reg}\ \ t\ \right] = \left[\dot{Q}_j^{reg}(t) - \dot{Q}_{j,steady}^{reg} \right] +$$
$$\int_0^t du \left[j_j^{in}\ \ u\ + \frac{\pi_j^{reg}\dot{Q}_j^{reg}\ u}{2} - \left[\frac{d < \ln p_j^{reg} >}{2\gamma_j^{reg} du} + \frac{dV_j^{reg}\ \ u}{2du} \right] \right] \left[\dot{Q}^{loop}\ \ u\ - M^{loop}\ \frac{d\left[h_j^{reg}\ \ u\ \right]}{du} \right] \quad (11)$$

Region j mass balance

$$\frac{d}{dt}\left[m_j^{region}(t) \right] = M^{loop} \int_0^t du \left[j_j^{in}\ \ u\ + \frac{\pi_j^{reg}\dot{Q}_j^{reg}\ u}{2} - \left[\frac{d < \ln p_j^{reg} >}{2\gamma_j^{reg} du} + \frac{dV_j^{reg}\ \ u}{2du} \right] \right] \frac{d\left[m_j^{region}(u) \right]}{du} \quad (12)$$

For unheated sections the same equations apply with null heat-flux.

6 Computation of volumetric flows

6.1 Volumetric flows

To close the system it is necessary to compute $j_k^{in}(t)$. As it is well known, a classical volume conservation (Herrero and Izquierdo, 2011) gives that

$$j_k^{out}(t) - j_k^{in}(t) = \pi_k \dot{Q}_k^{reg}(t) + \gamma_k \frac{dp_k}{dt} + \frac{dV_k}{dt} \tag{13}$$

$$\rho_{k+1} j_{k+1}^{in} = \rho_k j_k^{out} \qquad \rho_k = \frac{m_k}{V_k} \qquad \pi_k \equiv \left[\frac{\partial\ 1/\rho}{\partial h} \right]_p \qquad \gamma_k \equiv \left[\frac{\partial \ln \rho}{\partial \ln p} \right]_s$$

and the helium equation of state (EOS) provides the pressure as a function of enthalpy and density. In (Takeda et al., 2000) a second order Virial series describes helium as a real gas. The Virial format is the EOS format chosen in GASTEMP.

$$p == \frac{RT\rho}{Mol}\ 1 + B(T)\rho \qquad B\ T\ = 4.5x10^{-4} \left[\frac{m^3}{kg} \right] + \frac{5.42}{1890(^o K) + T} \left[\frac{m^3}{kg} \right] \tag{14}$$

Coefficients π_k, and γ_k are also determined from the EOS , the last being well approximated by a constant.

6.2 Pumps modelling

The above equations allow finding volumetric flows at all regions except the connection at the pump inlet and outlet, where the pump characteristics provide the alternate necessary information. According to (Takeda et al., 2000), in each pump.

$$\frac{p_{outlet}}{p_{inlet}} = a + b \left(\frac{G\sqrt{T_{inlet}}}{p_{inlet}} \right)^3 + c \frac{\omega^2}{T_{inlet}} \tag{15}$$

When combined with the EOS and mass conservation at the pump inlet, outlet

$$\frac{p_{outlet}}{p_{inlet}} = \frac{T_{outlet}\rho_{outlet}(1+B_{outlet}\rho_{outlet})}{T_{inlet}\rho_{inlet}(1+B_{inlet}\rho_{inlet})} = \frac{T_{outlet}\, j_{inlet}(j_{oulet}+B_{outlet}G)}{T_{inlet}\, j_{outlet}(j_{inlet}+B_{inlet}G)} \tag{16}$$

it provides the relation between the pump volumetric flows inlet and outlet for a given pump mass flow and angular velocity that are given as part of the transient scenario description

Fig. 6 shows a reasonable fit (using **Eq**. 16) to the Q-H characteristic curve of the primary and secondary helium circulators (Takeda et al., 2000).

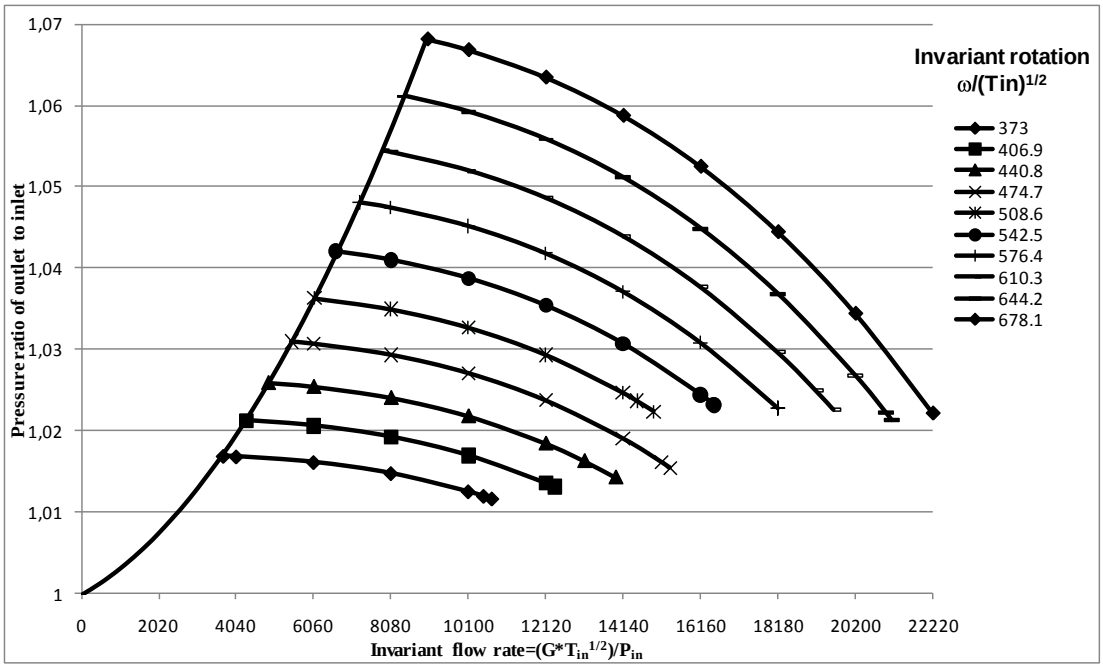

Fig. 6 Fit to the Q-H characteristic curve of primary and secondary helium circulators

7. Steady states.

It is important to ensure that success transients start and finish at a steady state. Damage transients should start at a steady state and finish when damage indicator process variables reach its safety limit.

7.1 Core steady states. Global balance

A steady reactor should be critical, so at steady states $\rho = 0$. Then, solving **Eq**. (10) for the initial state.

$$\left[A(0) x_{ss}^{ini} \right]_j + \frac{\delta_{j4} T_w^{ini}(0)}{R_{v\,He} C_v} = 0 \qquad \frac{x_j^{ini}(0)}{n^{ini}(0)} = -\frac{A(0)^{-1}_{j4}}{A(0)^{-1}_{14}} \qquad (17)$$

Eq. 17-takes into account that A(0) is singular, which implies that an initial power and sink temperature should be given and then the rest of the temperatures are obtained.

In the same way, those equations work at the final steady states, but now the final values should satisfy the reactivity balance given by **Eq**.3, that ,when integrated , gives the additional relation

$$\rho(\infty) - \rho(0) = \int_0^\infty dt \left[\frac{\partial \rho}{\partial T_f} \frac{\partial T_f}{\partial t} + \frac{\partial \rho}{\partial T_v} \frac{\partial T_v}{\partial t} + \frac{\partial \rho}{\partial Z_{bc}} \frac{\partial Z_{bc}}{\partial t} \right] = \sum_{k=3,4} \int_{x_k^{initial}}^{x_k^{final}} dx_k \frac{\partial \rho(x_k)}{\partial x_k} + \rho_{rod}^{out} - \rho_{rod}^{in} = 0 \qquad (18)$$

So, as indicated by **Figures** 3 and 4, the areas of the reactivity coefficients impose a constraint to the final values due to the reactivity feedback, which replaces the need to know the initial power.

7.2 Regions steady states.

At each region, we account for the fact that the steady state heat flux should equal the steady state power generation. So, once the initial and final steady values of the neutron power n, and heat sink temperature T_w are known through the global balance, they are used by the GASTEMP routines responsible of finding regional steady states.

8. Application .The rod withdrawal design basis transient

8.1 Transient scenario.

The following scenario description is given in the safety analysis report of the HTTR and it has been followed in our parallel GASTEMP/HTTR5 simulation: (Saito et al., 1994).

"It is assumed that a pair of CRs are abnormally withdrawn by a mis-operation from a subcritical condition during a reactor start-up. This transient would cause a reactor power increase and a fuel temperature raise with an abnormal insertion of the reactivity into the core. However, the operator will be able to recognize the abnormal state by monitoring instrumentation of various process parameters and take timely steps to ensure safety. When a reactor scram is required, the reactor will be scrammed by the reactor protection system and the residual heat will be removed by the ACS. Then this transient will terminate safely".

8.2 Conditions

"The following analytical conditions are applied to get reasonably conservative results. The reactor power is 10^{-7}% (0.03W) of the rated power (30MW). This is the equivalent to a power level generated by a neutron source. The primary coolant flow rate is assumed to be that for the high temperature test operation mode. The initial temperatures of the fuel, moderator and primary coolant are all assumed to be 200ºC as the most conservative value in the state of low power operation from the viewpoint of the temperature feedback effect. The reactivity coefficients used in the safety analysis are assumed to be the minimum value with respect to the temperatures of fuel and moderator, so that the peak core power might become maximum by the most conservative negative temperature reactivity feedback effect. The reactivity insertion rate by the CR withdrawal is assumed to be 1.2×10^{-6} $\Delta k/k/s$ which is the boundary reactivity between with and without a scram, and which gives the maximum fuel temperature"

8.3 Results

Fig. 7 and **Fig. 8** show the transients of the reactor power and the maximum fuel temperature,

using GASTEMP/HTTR5 and JAEA respectively.

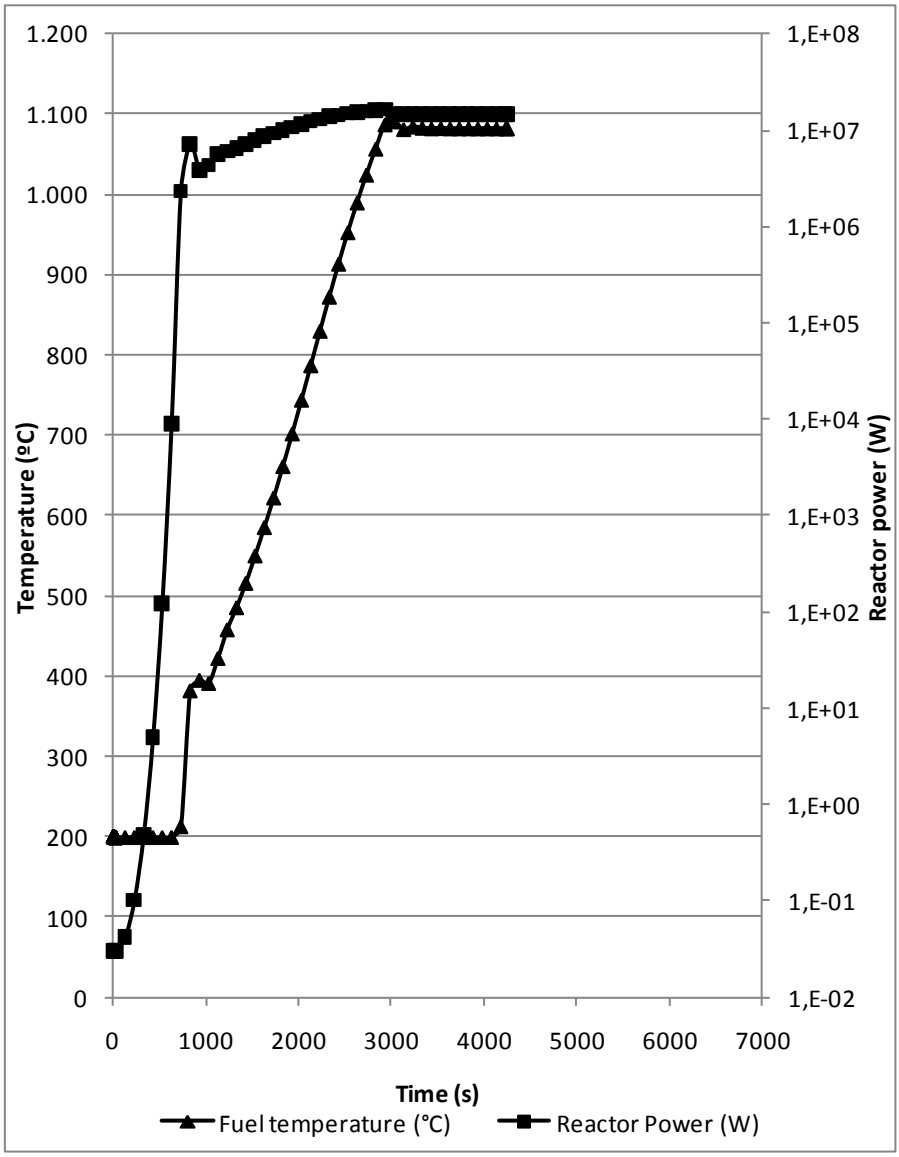

Fig. 7 Transient behaviour during abnormal control rod withdrawal during subcritical condition (GASTEMP/HTTR5)

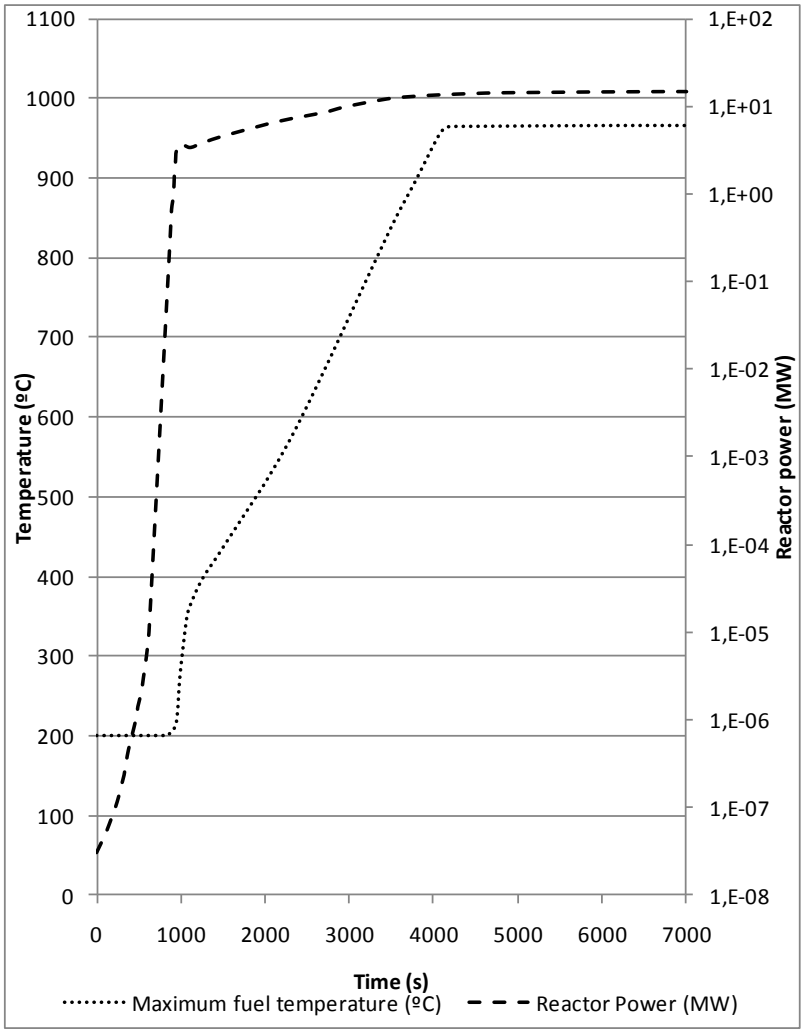

Fig. 8 Transient behaviour during abnormal control rod withdrawal during subcritical condition (JAERI) (Saito et al., 1994)

Despite the simplicity of the model, GASTEMP/HTTR5+ results are acceptable, the shape of the curves obtained are very similar to the JAEA results, and the stationary values are similar, in the case of HTTR5+ for the reactor power is 14.7 MW and in the case of the fuel temperature around 1080°C, the results of the JAEA are, for the reactor power around 14.5 MW and for the fuel temperature 965°C.

The GASTEMP/HTTR5+ simulates this transient in 9 seconds

9. Preliminary damage domain of the rod withdrawal transient.

Once the adequacy of the model has been shown, we now test its use for its primary purpose,

namely finding damage domains.

In **Fig.** 9 and **Fig.** 10 we present results of the damage domain that was obtained in case of failure of the trip system, either because the trip setpoint was not reached, or the trip system failed preventing the stop rods to drop (ATWS anticipated transient without scram).

We only considered the high neutron flux reactor trip setting, and included only the rod withdrawal speed and the overall reactivity insertion among the parameters. The initial situation was with the control bank totally inserted, as it corresponds to the low power test start-up operation. These results provide information about the sensitivity of the protection design to the neutron flux settings and the associated safety limit.

An initial random sampling of the parameters was performed. Pairs of parameter values were formed by taking random values from the variation range of each parameter, namely, from 1 mm/s to 70 mm/s for the bank speed and from 4.138E-6 to 1.2414E-5 for the differential bank worth.

The objective of the random sampling is to get an idea of the damage domain shape. Then, we use the parameter sweeping method using the information of the previous method. For each parameter, maximum, minimum and delta values are provided to the computer program. The process starts by calculating the transient with both parameters at their maximum values. Then, the bank worth is decreased by delta steps while maintaining the speed value. This process continues until getting a non-damage transient (i.e., reaching the boundary of the damage domain) or reaching the minimum worth value. The bank speed is then decreased by a delta step and the bank worth sweeping is restarted from its maximum value. The overall process ends when additional damage transients are not expected or when both parameters reach their minimum values(Hortal, 2012) .

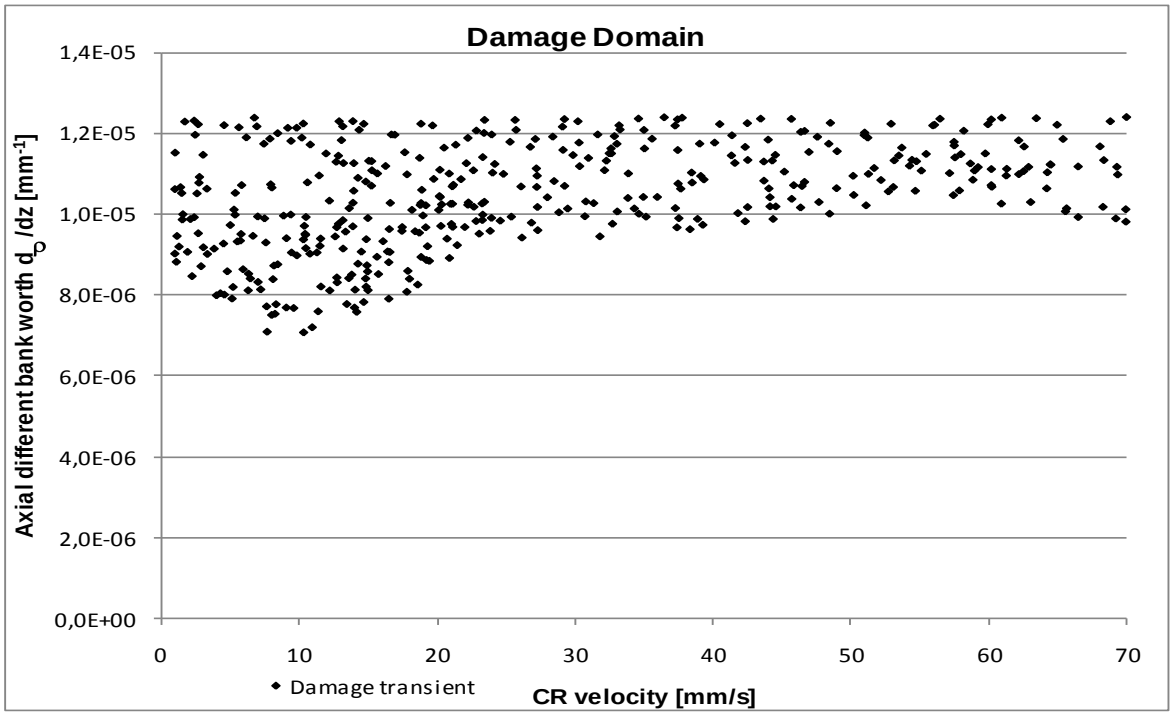

Fig. 9. Searching of damage domain using random sampling.

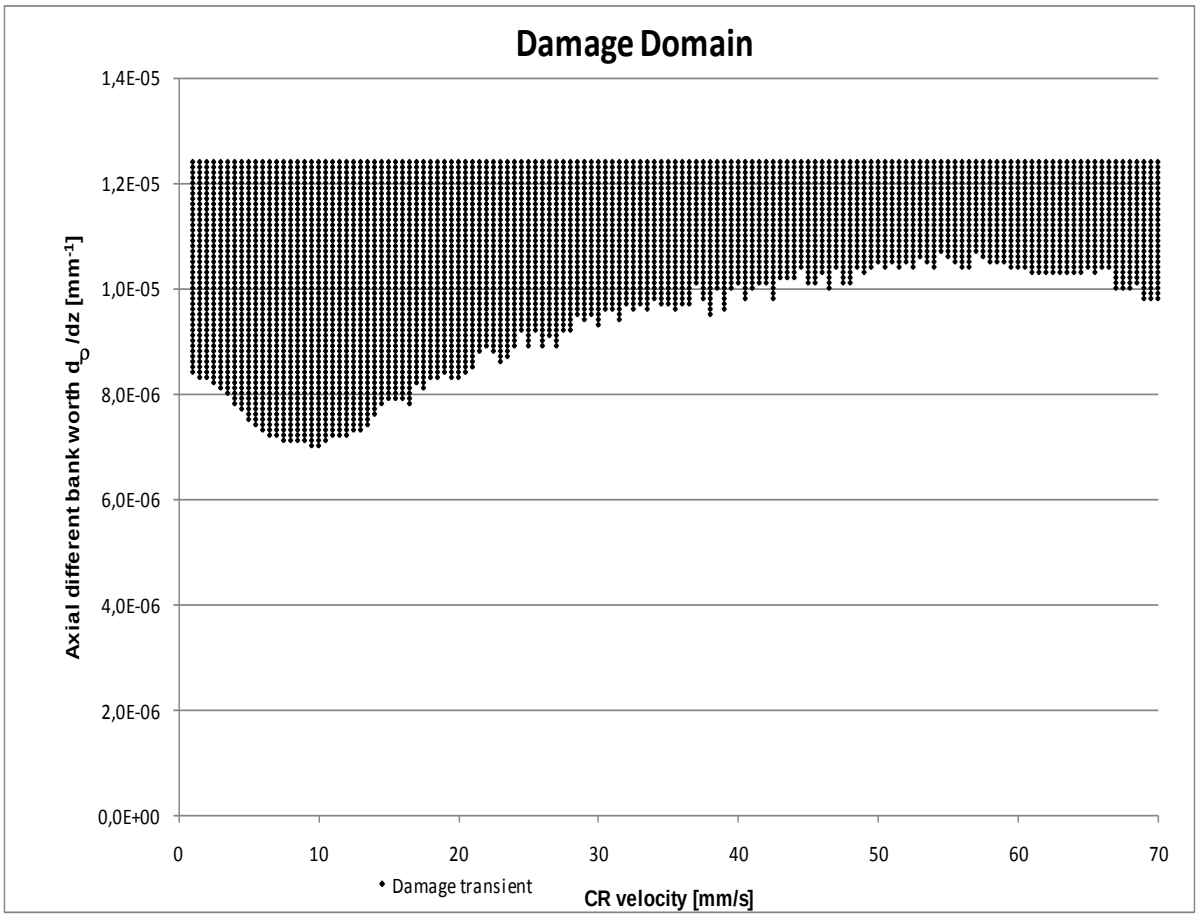

Fig. 10. Damage domain search result using a parameter sweeping method.

10 Conclusions

An adequate deterministic model with the capability to analyze damage domains related to the HTTR was described and has been applied to a rod withdrawal design basis transient.

The design transient was simulated with the objective to compare results of the HTTR5 with those obtained by the JAEA, showing adequate comparison.

The model was then applied to find the damage domain of this design basis transient, showing its efficiency. Different sampling methods were used to optimize the search. From these results, yet preliminary, the following may be concluded:

1. We confirm the consistency of the results when using two different sampling methods to generate the paths**.**
2. The results show that a minimum differential bank worth of 7.014E-6 is required to get damage, even if no reactor trip is actuated when required (ATWS).
3. No path was found in the damage domain without activating the high flux reactor trip signal, so the damage domain, is expected to have an out of design low frequency as it requires failure of the trip system.
4. There is a trade-off between bank differential worth and bank speed, the worse combination being at $\frac{\partial \rho}{\partial Z_{bc}} = 7.014E-6\left[mm^{-1}\right]$ $\frac{\partial Z_{bc}}{\partial t} = 10\left[\frac{mm}{s}\right]$, as a result of the reactivity feedback effects that control the transient into a final steady state.

More detailed information about these preliminary results will be given in subsequent papers.

Acknowledgements

This work has been developed in the frame of the project *"Advanced PSA methods for Reactor Independent Technology"* of the 2009 R+D Program on Nuclear Safety and Radiological Protection of the Nuclear Safety Council of Spain.

The authors wish to thank the HTTR-JAERI researchers, in particular to Dr. Tatsuo IYOKU and Dr. Takeschi TAKEDA for the quick response to our questions.

Appendix A

Special form of the thermo-fluid-dynamic balances in loops at high speed

General balance equations

The general balance equations of fluid mechanics may be given a special form when considering fluid loops with high velocity due the high capacity of the pumps. For any extensive property $\psi(z,t)$, a loop of length L implies that

$$\psi_j(z+L,t+\tau)=\psi_j(z,t+\tau) \tag{A.1}$$

so, if $\tau(z,t)$ represents the time it takes to traverse the loop starting at (z,t) and we assume it to be small enough

$$\psi_j(z,t+\tau)-\psi_j(z,t)\approx\tau(z,t)\frac{d\psi_j}{dt} \quad \text{(high velocity approximation)} \tag{A.2}$$

Then, the traditional transport balance

$$\frac{D_v\rho_j\psi_j}{Dt}=S_\psi \qquad \frac{D_v\rho_j\psi_j}{Dt}\equiv\left[\frac{\partial\rho_j\psi_j}{\partial t}+\frac{\partial\rho_j j\psi_j}{\partial z}\right]=\rho_j\left[\frac{\partial\psi_j}{\partial t}+\frac{\partial j\psi_j}{\partial z}\right] \tag{A.3}$$

may be average- integrated along the loop during time tau(z,t) so that

$$\frac{d\,M_j^{loop}\psi_j^{loop}}{dt}=S_\psi^{loop}=\frac{\partial M_j^{loop}\psi_j^{loop}}{\partial t}+\frac{(\rho_j j\psi)(z+L,t+\tau)-(\rho_j j\psi)(z,t)}{L}\approx\frac{\partial M_j^{loop}\psi_j^{loop}}{\partial t}+\frac{\tau(z,t)}{L}\frac{\partial G_j\psi_j}{\partial t} \tag{A.4}$$

where all quantities labelled loop mean the averages around it. So, we have that

$$\frac{\partial\left[G_j\psi_j\right](z,t)}{\partial t}=\frac{L}{\tau(z,t)}\left[S_\psi^{loop}(z,t)-\frac{\partial\left[M_j^{loop}\psi_j^{loop}\right](z,t)}{\partial t}\right] \tag{A.5}$$

and

$$\left[G_j\psi_j\right](z,t)-\left[G_j\psi_j\right](z,0)=\int_0^t du\,\frac{L}{\tau(z,u)}\left[S_\psi^{loop}(z,u)-\frac{\partial\left[M_j^{loop}\psi_j^{loop}\right](z,u)}{\partial u}\right] \tag{A.6}$$

Global Loop balance

A global balance in the loop gives that

$$\frac{1}{L}\int_0^L dz\left[S_\psi^{loop}(z,t)-\frac{\partial\left[M_j^{loop}\psi_j^{loop}\right](z,t)}{\partial t}\right]=w_j^{in}\psi_{in}-w_j^{out}\psi_{out} \qquad \text{(A.7)}$$

$$M_j^{loop}\frac{\partial}{\partial t}\frac{1}{L}\int_0^L dz\left[\psi_j^{loop}(z,u)\right]=w_j^{in}\psi_{in}-w_j^{out}\psi_{out}+\frac{1}{L}\int_0^L dz\left[S_\psi^{loop}(z,u)\right] \qquad \text{(A.8)}$$

where w_j^{in}, w_j^{out} and ψ_{in}, ψ_{out} are the flow mass in and out of the loop and their transported properties.

Regional balances

On the other hand, the classical balance in one given portion of the loop gives

$$m_j^{region}\frac{\partial}{\partial t}\left[\psi_j^{region}(t)\right]=G_j^{region,in}\psi_{in}^{region}-G_j^{region,out}\psi_j^{region,out}+S_\psi^{region}+\left[w_j^{in}\psi_{in}-w_j^{out}\psi_{out}\right]_{region} \text{(A.9)}$$

and using **Eq.** A.4 assuming no flow out of the loop in the region

$$m_j^{region}\frac{\partial}{\partial t}\left[\psi_j^{region}(t)\right]=S_\psi^{region}+\left[G_j^{region,in}\psi_{in}^{region}-G_j^{region,out}\psi_j^{region,out}\right]_{steady}+ \\ +1/L_{region}\int_0^t du\int_{region} dz\; j(z,t)\left[S_\psi^{loop}(z,u)-M_j^{loop}\frac{\partial\left[\psi_j^{loop}\right](z,u)}{\partial u}\right] \qquad \text{(A.10)}$$

where we have also made the approximation $\frac{L}{\tau(z,u)}=j(z,t)$ with $j(z,t)$ the fluid velocity. For large values of t compared with the loop times, we may approximate

$$\psi_j^{region}(t)\approx\psi_{j,region}^{loop}(t) \qquad m_j^{region}(t)\approx m_j^{loop}(t) \qquad S_{j,region}^{loop}(t)=\sum_j S_j^{region}(t) \qquad \text{(A.11)}$$

On the other hand

$$\int_{region} dz\, j(z,u)F(z,u) = j_{out}(u)\int_{region} F(z,u) - \int_{region} dz \frac{\partial}{\partial z} j(z,u) \int_0^z F(z,u)$$
$$\simeq \left[j_{out}(u) - \frac{1}{2}\left[\frac{\partial}{\partial z} j(z,t) \right]_{reg} \right] F^{reg}(u) \qquad \text{(A.12)}$$

$$\frac{\partial}{\partial z} j(z,t) = \pi(z,t)Q(z,t) - \frac{1}{\gamma(z,t)}\left[\frac{d}{dt} \ln p(z,t) + \frac{d}{dt} V(z,t) \right] \qquad \text{(A.13)}$$

and using the properties of the steady state and reincorporating the flows in-out the loop, we get the special form of the balance

$$m_j^{region} \frac{\partial}{\partial t}\left[\psi_j^{region}(t) \right] = \left[S_{\psi}^{region}(t) - S_{\psi,steady}^{region} \right] + w_j^{regin}\psi_{in} - w_j^{regout}\psi_{out} +$$
$$\int_0^t du \left[j^{in}(u) + \frac{\pi_{reg}Q_{reg}(u)}{2} - \frac{d < \ln p_{reg} >}{2\gamma_{reg}du} - \frac{dV_{reg}(u)}{2du} \right] \left[S_{\psi,region}^{loop}(u) - M_j^{loop} \frac{\partial\left[\psi_j^{region}(u) \right]}{\partial u} \right] \qquad \text{(A.14)}$$

Appendix B

-Core heat flux and its coupling to GASTEMP

The system showed in section 3, composed by **Eq.** (1), **Eq**. (5), and **Eq**. (6) could be represented as,

$$\dot{x}(\rho(t),t) = H(\rho(t))x(\rho(t),t) + \frac{\delta_{j4}}{C_v R_v} T_{He}(t) \tag{B.1}$$

with

$$H(\rho) = \begin{bmatrix} \frac{\rho-\beta}{\Lambda} & \lambda & 0 & 0 \\ \frac{\beta}{\Lambda} & -\lambda & 0 & 0 \\ \frac{1}{C_f} & 0 & -\frac{1}{C_f \ \ R_f + R_g} & \frac{1}{C_f \ \ R_f + R_g} \\ 0 & 0 & \frac{1}{C_v \ \ R_f + R_g} & -\frac{R_v + R_f + R_g}{C_v R_v \ \ R_f + R_g} \end{bmatrix} * \begin{bmatrix} n \\ C \\ T_f \\ T_v \end{bmatrix} \tag{B.2}$$

with a solution

$$x_j(\rho,t) = \sum_k \left[\exp \ \ H(\rho) \ \ t \right]_{jk} x_k(0) + \int_0^t \left[\exp \ \ H(\rho) \ \ (t-u) \right]_{j4} \frac{T_{He}(u)}{C_v R_v} \tag{B.3}$$

For j=4 $x_4(\rho,t) = T_v(\rho,t)$

$$T_v(\rho,t) = \sum_k \left[\exp \ \ H(\rho) \ \ t \right]_{4k} x_k(0) + \left[\int_0^\Delta + \int_\Delta^t \right] \left[\exp \ \ H(\rho) \ \ u \right]_{44} \frac{T_{He}(t-u)}{C_v R_v} \tag{B.4}$$

and the heat flux is

$$\frac{T_v(\rho,t)-T_{He}(t)}{R_{v\,He}}=\frac{1}{R_{v\,He}}\left[\frac{\Delta\left[1+\frac{\Delta}{2}H_{44}\right]}{C_vR_{v\,He}}-1\right]T_{He}(t)+$$

$$+\frac{1}{R_{v\,He}}\sum_k\left[\exp\quad H(\rho)\quad t\right]_{4k}x_k(0)+\frac{1}{R_{v\,He}C_vR_v}\int_0^{t-\Delta}du\left[\exp\quad H(\rho)\quad (t-u)\right]_{44}T_{He}(u)\quad \text{(B.5)}$$

where Δ is a time step such that

$$\left[\exp\quad H(\rho)\quad u\right]_{44}\cong 1+H_{44}u=1-\frac{R_v+R_f+R_g}{C_vR_v\quad R_f+R_g}u \qquad \text{(B.6)}$$

Eq B.5 provides the heat flux at time t as a function of the fluid temperature at the same time, as required to couple it to GASTEMP . The integrals are computed with efficient conventional methods involving past time history, so already known at time t.

The same technique is applied to the heat exchanger heat flux and to the global balance, in this case replacing T_{He} by T_w and matrix H by A in **Eq.** 10 of the main text.

Figure captions

Fig.1 Reactor cooling system of HTTR (Saito et al., 1994).

Fig.2 Schematic diagram of the reactor cooling system of HTTR.

Fig.3 Doppler coefficient.

Fig.4 Temperature coefficient of moderator.

Fig.5 Cross section of a fuel element and heat transfer tube

Fig.6 Fit to the Q-H characteristic curve of primary and secondary helium circulators

Fig.7 Transient behaviour during abnormal control rod withdrawal during subcritical condition HTTR5+

Fig.8 Transient behaviour during abnormal control rod withdrawal during subcritical condition JAERI

Fig. 9. Searching of damage domain using random sampling.

Fig. 10. Searching of damage domain using a parameter sweeping.

References

Benikhlef T., Benazzouz D., Izquierdo J.M., Sanchez M., (2011), Damage domains of chemically reacting industrial facilities. An adequate identification model for Bhopal-like scenarios. Asia-Pacific Journal of Chemical Engineering.

EPRI, (2011), Technical Framework for Management on Safety Margins--Loss of Main feedwater Pilot Application. EPRI, Palo Alto, CA.

Fujimoto N., Nojiri N., Ando H., Yamashita K., (2004), Nuclear design. Nuclear Engineering and Design 233, 23-36.

GIF, (2002), A technology roadmap for generation IV nuclear energy systems. U.S. DOE Nuclear Energy Research Advisory Committee and the Generation IV International Forum, p. 91.

Herrero R.H., Izquierdo J.M., (2011), Development of a computer tool for in-depth

analysis and post processing of the RELAP5 thermal hydraulic code. NUREG/IA-0253. US Nuclear Regulatory Commission. Office of Nuclear Regulatory Research.

Hittner D., Bogush E., Besson D., Buckthorpe D., Chauvet V., Fütterer M.A., Van Heek A., Von Lensa W., Phélip M., Pirson J., Scheuermann W., Verrier D., (2006), RAPHAEL, a Europeam project for the development of HTR/VHTR technology for industrial process heat supply and cogeneration Third International Topical Meeting on High Temperature Reactor Technology, Johannesburg, South Africa, p. 10.

Hortal J., (2012), Schematic Example for Comparison of Uncertainty Analysis Methods. Nuclear Safety Council (Spain), Madrid.

Iyoku T., Ueta S., Sumita J., Umeda M., Ishihara M., (2004), Design of core components. Nuclear Engineering and Design 233, 71-79.

Izquierdo J.M., Cañamon I., (2008), TSD, a SCAIS suitable variant of the SDTPD, ESREL, Valencia, Spain.

Izquierdo J.M., Cañamón I., (2006), Status report on dynamic reliability: SDTPD path and sequence TSD developments. Application to the WP5.3 benchmark Level 2 PSA exercise. SARNET-PSA2 WP5.3 D73.

Izquierdo J.M., Hortal J., Sánchez M., Meléndez E., Herrero R., Gil J., Gamo L., Fernández I., Esperón J., González P., Queral C., Expósito A., Rodríguz G., (2008), SCAIS (Simulation Code System for Integrated Safety Assessment): Current status and applications, in: Martorell (Ed.), Safety, Reliability and Risk Analysis: Theory, Methods and Aplications, ESREL 2008. Taylor & Francis Group, Valencia, Spain, p. 3510.

Izquierdo J.M., Queral C., Herrero R., Hortal J., Sanchez M., Melendez E., Muñoz R., (2001), Role of fast running TH codes and their coupling with PSA tools, OECD/CSNI workshop on advanced thermal hydraulica and neutronic codes current and future applications, Spain, Barcelona.

Izquierdo J.M., Sanchez M., (2007), GASTEMP: a SCAIS Module for the modelling of chemical reactions in a gas mixture. Nuclear Safety Council (Spain).

Kunitomi K., Nakagawa S., Shiozawa S., (2004), Safety evaluation of the HTTR. Nuclear Engineering and Design 233, 235-249.

Labeau P.E., Izquierdo J.M., (2005a), Modeling PSA problems - I. The Stimulus driven theory of probabilistic dynamics (SDTPD). Nuclear Science and Engineering 150, 115-139.

Labeau P.E., Izquierdo J.M., (2005b), Modeling PSA problems - II. A cell-to-cell transport theory approach. Nuclear Science and Engineering 150, 140-154.

Saito S., Tanaka T., Sudo Y., Baba O., Shindo M., Shiozawa S., Mogi H., Okubo M., Ito N., Shindo R., Kobayashi N., Kurihara R., Hayashi K., Hada K., Kurata Y., Yamashita K., Kawasaki K., Iyoku T., Kunitomi K., Maruyama S., Ishihara M., Sawa K., Fujimoto N., Murata I., Nakagawa S., Tachibana Y., Nishihara T., Oshita S., Shinozaki M., Takeda T., Sakaba S., Saikusa A., Tazawa Y., Fukaya Y., Nagahori H., Kikuchi T., Kawaji S., Isozaki M., Matsuzaki S., Sakama I., Hara K., Ueda N., Kokusen S., (1994), Design of High Temperature Engineering Test Reactor (HTTR). JAERI, p. 247.

Sánchez M., Izquierdo J.M., Hortal J., Melendez E., Fernandez I., Gil J., Murcia S., Gomez J., Queral C., Expósito A., Rodríguz G., Ibañez L., (2009), Proposal for a Suitable Strategy of Exceedance Frequency Computation. Implementation on SCAIS Simulation-Based Safety Code Cluster, In Proc. Int. Conf. Nuclear Energy for New Europe NENE2009, Bled, Slovenia.

Sumita J., Ishihara M., Nakagawa S., Kikuchi T., Iyoku T., (2004), Reactor internals design. Nuclear Engineering and Design 233, 81-88.

Takeda T., Nakagawa S., Tachibana Y., Takada E., Kunitomi K., (2000), Analytical Evaluation on Loss of Off-Site Electric Power Simulation of the High Temperature Engineering Test Reactor. JAERI, p. 78.

List of acronyms

ACS	Auxiliary cooling system
AGC	Auxiliary gas circulator
AHX	Auxiliary heat exchanger
AOO	Anticipated operational occurrence
ATWS	Anticipated transient without scram
CR	Control rod
DBEP	Design basis envelop
HTTR	High Engineering Test Reactor
IHX	Intermediate heat exchanger
JAEA	Japan Agency of Energy Atomic
LCO	Limiting conditions for operation
LSSS	Limiting safety system settings
ODE	Ordinary differential equations
PCS	Primary cooling system
PGC	Primary gas circulator
PPWC	Primary pressurized water cooler
PRMS	Power range monitoring system
PWCS	Pressurized water cooling system
SGC	Secondary gas circulator
SHCS	Secondary helium cooling system
SPWC	Secondary pressurized water cooler
TSD	Theory of stimulated dynamics
VCS	Vessel cooling system

Nomenclature

Symbol	Description	Units
β	Fraction of delayed neutrons	
C_v ,C_p	Heat Capacity at constant volume or pressure	J/K
Z_{bc}	Control rod position	m
j	Volumetric flow	m^3/s
T_f	Fuel temperature	ºC
T_v	Cladding temperature	ºC
T_{He}	Helium temperature	ºC
λ	Decay constant	s^{-1}
Λ	Mean generation time	s
C	Precursors power	W
q	Neutron source	W
G	Flow rate	kg/s
n	Neutron power	W
p_{inlet}	Pressure at pump inlet	MPa
p_{outlet}	Pressure at pump outlet	MPa
ρ	Reactivity	
ω	Pump rotation speed	min^{-1}
T_{inlet}	Temperature inlet	C
ss	steady state	
n_d	steady power prior to the transient	W
P_d	Fission product decay heat	W
t_s	Elapsed time after scram	s
P_{act}	Decay heat of actinide	W

Symbol	Description	Value
Q	Average energy released per fission	200MeV
E_U	Average energy released by decay of ^{239}U	0.474MeV
E_{Np}	Average energy released by decay of ^{239}Np	0.419MeV
λ_{Np}	Decay constant of ^{239}Np	$3.41\text{x}10^{-6}$MeV
λ_U	Decay constant of ^{239}U	$4.91\text{x}10^{-4}\text{s}^{-1}$
R	Generation ratio of ^{239}U during reactor operation	0.636

Parameter	Value
a	0.9935665
b	$-2.094E^{-4}\left[\frac{s}{K^{1/2}m^2}\right]^3$
c	$6.09E^{-4}\left[Ks^2\right]$